CHEMISTRY
A European Journal

Accepted Article

Authors: Elif Pınar Alsaç, Emine Ülker, Satya Vijaya Kumar Nune, Yavuz Dede, and Ferdi Karadas

FULL PAPER

Tuning Electronic Properties of Prussian Blue Analogues for Efficient Water Oxidation Electrocatalysis: Experimental and Computational Studies

Elif Pınar Alsaç, [a] Emine Ülker, [d] Satya Vijaya Kumar Nune, [a] Yavuz Dede, [c]* Ferdi Karadas[a], [b] *

Abstract: While several Prussian blue analogues (PBAs) have been investigated as water oxidation catalysts, the field lacks a comprehensive study that focuses on the design of the ideal PBA for efficient water oxidation catalysis. Herein, a series of PBAs with different cyanide precursors were investigated to study the effect of hexacyanometal group to their electrocatalytic water oxidation activities. Cyclic voltammetric, chronoamperometric, and chronopotentiometric measurements reveal the close relation between the electron density of electroactive cobalt sites and electrocatalytic activity, which is also confirmed by Infrared and XPS studies. pH dependent cyclic voltammetry and computational studies were also performed to gain insight about the catalytic mechanism and electronic structure of cyanide-based systems to identify possible intermediates and to assign the rate-determining step of the target process.

Introduction

Increase in energy demand has forwarded scientific community, particularly in the last two decades, to find alternative energy sources that will replace limited fossil-based fuels.[1] Since solar energy that utilizes the production of H_2 from water has been one of the most promising candidates among sustainable sources of energy, much effort has recently been devoted to investigate efficient methods to split water.[2–7] Since water splitting process is mostly limited by the high overpotential of oxygen evolution reaction (OER), many studies have been performed to introduce novel catalysts that operate at low overpotentials.[8] Many inorganic systems including metal oxides,[9–12] perovskites,[13–15] amorphous materials,[16] noble-metal based materials,[17,18] and metal organic frameworks (MOFs)[19,20] have been investigated as WOCs. Of these, cobalt oxides stand forward due to their high catalytic activities.[21,22] Despite their high catalytic activities, cobalt oxides have mainly

[a]   E. P. Alsaç, Dr. S.V.K. Nune, Prof. F. Karadas Department of Chemistry, Bilkent University, 06800 Ankara (Turkey) E-mail: karadas@fen.bilkent.edu.tr

[b]   Prof. Dr. F. Karadas UNAM-Institute of Materials Science and Nanotechnology Bilkent University, 06800 Ankara, (Turkey)

[c]   Prof. Y. Dede, Faculty of Science, Department of Chemistry, Gazi University 06500, Ankara (Turkey)
       dede@gazi.edu.tr

[d]   Prof. E. Ülker Department of Chemistry, Faculty of Arts & Sciences, Recep Tayyip Erdogan University, 53100, Rize (Turkey)

       Supporting information for this article is given via a link at the end of the document

two disadvantages;[23,24] i) low stability and high tendency to decompose in acidic medium, ii) difficulty in correlation of the catalytic activities with structure due to their amorphous nature. Non-oxide materials have also drawn attention as WOCs due to their favorable characteristics such as ease of preparation, stability at a wide range of pH, and robustness during catalytic processes.[25] Patzke et al. reported a carbodiimide-based material that could be used as a WOC, which is stable in acidic and neutral media.[26] A similar class of materials, metal dicyanamides, has also shown to be promising candidates for water oxidation electrocatalysis.[27] Cobalt hexacyanoferrates, members of Prussian blue analogue (PBA) family, are also exceptional candidates for electrocatalytic water oxidation due to their high catalytic activities, robustness, and stability at neutral pH.[28–30] A further study by Patzke et al. showed that PBAs can also be used for light driven water oxidation process in the presence of $[Ru(bpy)_3]^{2+}$ as a chromophore.[31] Despite their high turnover frequencies (TOFs), one of the main drawbacks of cyanide-based systems is their low concentration of electroactive cobalt sites. Their low concentration is attributed to the relatively larger distances between Co(II) sites (~10 Å) compared to oxide-based systems (~3 Å).[28] This problem has recently been overcome by our group with the use of a novel pentacyanoferrate-bound polymer as a precursor for Co-Fe PBAs, which resulted in a dramatic decrease in the crystallinities of PBAs, and thus, a significant increase in the surface concentration.[32] Galán-Mascarós et al. approached the same problem by using a new synthetic method for the preparation of thin films of PBAs, which involves chemical etching of cobalt oxides with a hexacyanoferrate solution to form an in situ PBA film. This novel method led to an impressive improvement on the stability of the electrode and electrocatalytic performance in a wide range of pH. It exhibits a much lower overpotential (510 mV) to obtain a current density of 1 mA cm^{-2}.[33] In addition, Fukuzumi et al. investigated the photocatalytic water oxidation performances of a series of Co-Pt PBAs in the presence of well-defined $Ru(bpy)_3^{2+}/S_2O_8^{2-}$ couple. The systematic study performed with $[Co(CN)_6]^{3-}$ and $[Pt(CN)_6]^{4-}$ groups in different stoichiometric ratios clearly showed that number of active sites is highly dependent on the number of defects.[34,35] Fukuzumi and coworkers also studied the effect of counter cation to the catalytic activity and quantum efficiency displayed by Co-Co PBAs in photocatalytic water oxidation process showing that a quantum efficiency of 200% can be achieved with Co-Co PBAs incorporating calcium ions as counter cations.[36] Previous studies mentioned above clearly show that slight modifications in the structure of PBAs could lead to a significant increase in their catalytic activities. Although previous studies took advantage of rich and well-established cyanide chemistry no study has been performed to investigate the effect of

hexacyanometal unit to the electronic properties and catalytic performance of electroactive cobalt sites. Herein, electrocatalytic measurements on a series of cobalt hexacyanometalates (CHCMs) incorporating different $M(CN)_6$ units (M = Co^{III}, Cr^{III}, $Fe^{II/III}$, and) together with characterization studies were performed to investigate the effect of the type and oxidation state of the metal in $M(CN)_6$ unit to the catalytic activity of PBAs. The effect of hexacyanometal group to the electronic properties of electroactive cobalt site was further examined with electronic structure calculations employing Density Functional Theory (DFT).[37,38]

Results and Discussion

Electrochemistry

All the electrochemical experiments were conducted with a PBA modified fluorine-doped tin oxide (FTO) electrode. Cyclic Voltammograms (CVs) of $Co[M(CN)_6]$ (M:Co^{III}, Cr^{III}, and $Fe^{II/III}$) were taken in a phosphate buffer with 1 M KNO_3 as the electrolyte in a 0.2–1.7 V vs. NHE potential range (Figure 1). [Co^{II}-Co^{III}] exhibits a quasi-reversible redox couple with an oxidation peak at 1.210 V and a reduction one at 1.031 V vs. NHE that can be assigned to Co^{2+}/Co^{3+} redox couple. A similar redox couple was observed also for other PBAs. Another peak, at a more positive potential, is observed at around 1.415 V vs. NHE for [Co^{II}-Co^{III}], which can be assigned to Co^{3+}/Co^{4+} redox process.[39] Tafel plots of each catalyst were obtained by performing chronoamperometry measurements at different applied potentials to further investigate their electrocatalytic performances. A linear trend was obtained between the logarithm of the steady state current densities and in an overpotential range of 283–483 mV with Tafel slopes in 90–130 mV dec^{-1} range (Figure 2). Tafel slopes obtained with [Co^{II}-Fe^{II}] and [Co^{II}-Fe^{III}] are slightly higher than those reported previously by Galan- Mascarós et al.[28,33] The difference is mainly attributed to different preparation methods since PBA modified electrodes prepared via an in situ method exhibit lower Tafel slopes (~ 90 mV dec^{-1}) compared to those prepared with drop casting.[26,32]

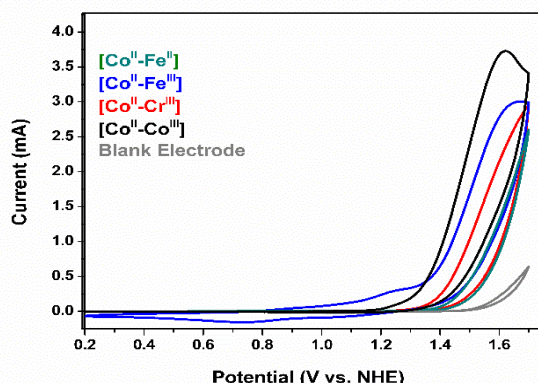**Figure 1.** Cyclic Voltammograms of PB derivatives ([Co^{II}-Co^{III}] black, [Co^{II}-Cr^{III}] red, [Co^{II}-Fe^{III}] blue, and [Co^{II}-Fe^{II}] green lines) in 50 mM KPi electrolyte at pH 7 with 50 mv sec^{-1} sweep rate. The gray line indicates the electrochemical response of blank electrode.

Similarity in the Tafel slopes indicates similar OER mechanisms. According to chronoamperometric measurements onset overpotentials of 283, 303, 323, and 343 mVs are obtained, respectively, for [Co^{II}-Co^{III}], [Co^{II}-Cr^{III}], [Co^{II}-Fe^{III}], and [Co^{II}-Fe^{II}], which are in line with cyclic voltammetric studies (Figure S1). Surface coverage of the electroactive Co^{2+} species on FTO electrode i.e., surface concentration, was determined by performing CVs at different scan rates (25–225 mV sec^{-1} range) recorded in the 0.8–1.6 V range. Surface concentration of derivatives were obtained in the 2–5 nmol cm^{-2} range, which is in good agreement with the previously reported studies (Figure S2).[28,32]
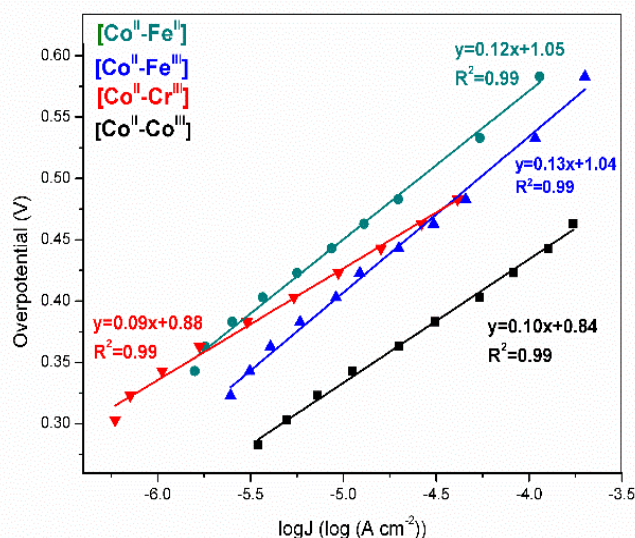

Figure 2. Tafel plots for PB derivatives from 1.1 to 1.4 V vs NHE recorded in a 50 mM KPi buffer at Ph 7.0.

Surface concentration was used to assess turnover frequencies (TOFs) of PBAs. TOFs at an overpotential of 400 mV were obtained as 5.0×10^{-2} s^{-1}, 3.0×10^{-3} s^{-1}, 4.4×10^{-3} s^{-1}, and 5.0×10^{-3} s^{-1} for [Co^{II}-Co^{III}], [Co^{II}-Fe^{II}], [Co^{II}-Fe^{III}], and [Co^{II}-Cr^{III}] (Figure S3). A comparison of TOFs, thus, shows that Co(II) sites available in [Co^{II}-Co^{III}] exhibit the highest catalytic activity. Chronopotentiometry (CP) has been performed to monitor the overpotential required to obtain a current density of 1 mA cm^{-2} during a 2h experiment. The overpotential for [Co^{II}-Co^{III}], decreases slightly at first and then maintains a constant overpotential while it increases gradually until stabilization for other PBAs. The observed overpotentials for 1 mA cm^{-2} are slightly higher than the ones extracted from Tafel slopes due to the formation of O_2 bubbles on the electrode surface during the measurement. CP studies show that [Co^{II}-Co^{III}] exhibits the lowest overpotential and η_{1mA} is determined to be 531, 578, 661, and 692 mVs for [Co^{II}-Co^{III}], [Co^{II}-Cr^{III}], [Co^{II}-Fe^{III}], and [Co^{II}-Fe^{II}], respectively (Figure 3).

Table 1. Summary of electrochemical properties for PBAs

Compound	$Co^{2+/3+}$ (mV)	V (CN) (cm^{-1})	TOF (η = 400 mV)	Surface Concentration (nmol cm^{-2})	$\eta_{1 mA}$ from Tafel Plot (mV)	Tafel Slope (mV dec^{-1})	$\eta_{1 mA}$ from CP (mV)	η_{onset} (CV)
[Co^{II}-Co^{III}]	1.010	2176	5.0×10^{-2}	4.11	531	99	565	283
[Co^{II}-Cr^{III}]	1.084	2173	5.0×10^{-3}	3.90	578	96	598	303
[Co^{II}-Fe^{III}]	1.084	2120	4.4×10^{-3}	5.48	661	127	717	323
[Co^{II}-Fe^{II}]	0.995	2072	3.0×10^{-3}	2.00	692	121	1079	343
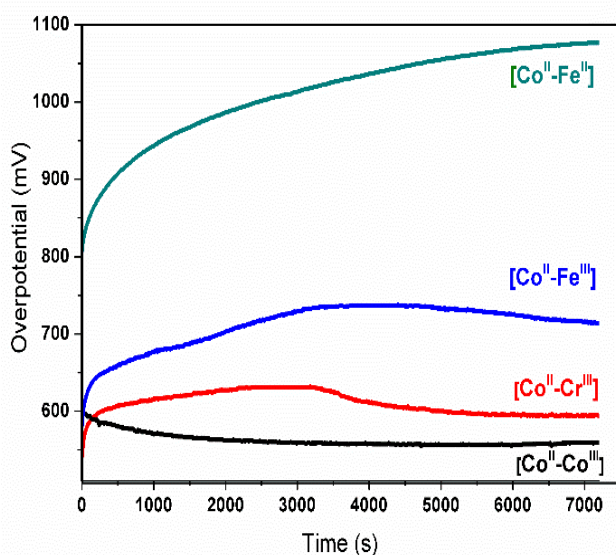
Figure 3. Chronopotentiometry measurement of PB derivatives at 1 mA cm^{-2} in a 50 mM KPi buffer at pH 7.0

Long term chronoamperometric studies at an applied potential of 1.4 V vs NHE were performed to investigate the stability of the PBA modified electrodes. The current density for each catalyst decreases until it reaches a constant value as previously reported by our group and Galán-Mascarós et al.[28,32]

The same trend can be obtained for four repeating cycles and the close similarity of cyclic voltammetric profiles obtained after each cycle indicates that catalysts retain their structure even during long term catalytic processes (Figure S4). An interesting anomaly is observed only for [Co^{II}-Cr^{III}] where a decrease in current density is obtained as usual followed by an abrupt increase after around 10 hours. A comparison of the CVs obtained before and after a 24 h electrolysis experiment indicates a significant increase in the onset overpotential and catalytic current density, which could be attributed to the decomposition of [Co^{II}-Cr^{III}] to a more catalytically active species.

Our characterization studies, which will be discussed in the following section also suggest that the decomposition occurs only during long-term electrolysis studies (longer than 10 h). Furthermore, a similar electrolysis study equipped with an O_2 probe has been performed with [Co^{II}-Co^{III}] to investigate the origin of current density and Faradaic efficiency. The perfect match between the theoretical yield obtained from chronocoulometry measurement and the experimental one obtained from O_2 probe indicates that the only origin of current density is catalytic water oxidation to O_2 evolution process and there are no competing redox reactions (Figure S5).

Characterization Studies

All samples are isostructural with Prussian Blue crystal structure adopting face-centered cubic structure (fcc) with Fm3m space group as confirmed by powder XRD studies. The characteristic 2theta (2θ) peaks for Prussian Blue have been observed for all of the materials (Figure S6) and lattice parameter was determined to be around 10 Å for each derivative (Table S1). XRD analysis in gracing incidence mode was also performed on the catalysts deposited on FTO before (pristine) and after (post-catalytic) the electrocatalytic studies to investigate the structural stability of catalyst during electrocatalysis. No additional peaks were observed in the XRD of post-catalytic samples and the peaks corresponding to Prussian Blue type structure remain confirming the stability of catalysts (Figure 4). The atomic ratio of metals in each compound was extracted by EDX analysis (Table S2). The following molecular formulae were obtained based on stoichiometric ratio of metals: $K_{0.76}Co_{2.62}[Co(CN)_6]_2$, $K_{0.82}Co_{2.59}[Cr^{III}(CN)_6]_2$, $K_{0.62}Co_{2.69}[Fe^{III}(CN)_6]_2$, and $K_{1.40}Co_{3.30}[Fe^{II}(CN)_6]_2$ for [Co^{II}-Co^{III}], [Co^{II}-Cr^{III}], [Co^{II}-Fe^{III}], and [Co^{II}-Fe^{II}], respectively. Each compound has similar potassium content in the 0.6-0.8 range, which results in an average of ~4.5 CN groups per Co(II) sites. The remaining coordination sphere of Co(II) sites are occupied by water molecules, which play active role in water oxidation (Figure S7).
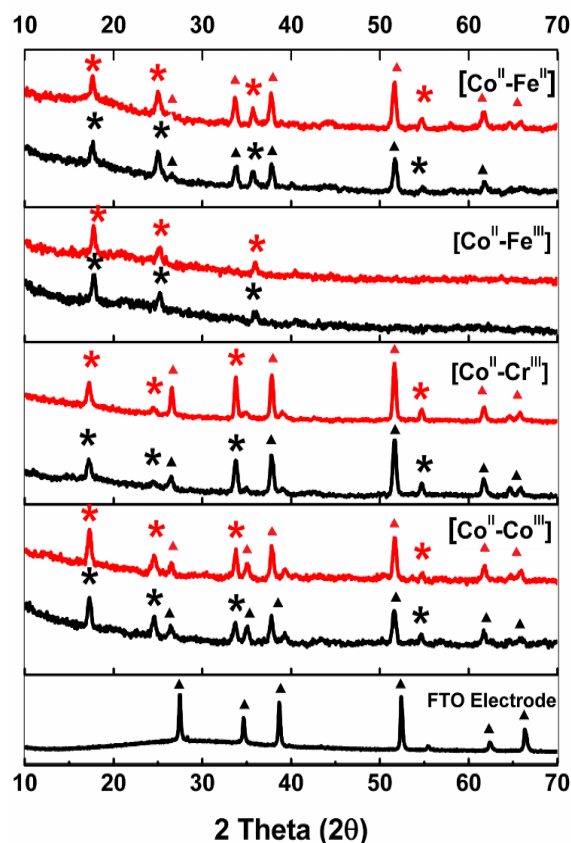
Figure 4. GI- XRD patterns of PB derivatives for pristine (black lines) and post catalytic (red lines). The peaks that belong to FTO electrode are marked with triangle (▲) and the peaks belong to Prussian Blue are marked with asterisk (*).

Infrared studies show that PBAs exhibit the characteristic bands that are observed for Prussian blue type systems; a) a sharp band at around 1610 cm^{-1} and a broad one at 3200–3500 cm^{-1}, which represent H-OH bending and OH stretch, respectively, b) a sharp peak at around 490–590 cm^{-1} due to M-C stretch, and c) a sharp stretch at around 2120–2180 cm^{-1} that is attributed to CN stretch (Table S3). PBAs exhibit higher CN stretching frequencies compared to their hexacyanometal precursors, which confirm the binding of nitrogen atoms of cyanide to Co(II) sites[28,40] (Figure S8). The Infrared analysis was also performed on the post-catalytic samples. The close similarity between the infrared spectra of cyanide stretches of pristine and post catalytic samples suggests that catalysts M-CN-Co^{II} type coordination mode is preserved during electrolysis (Figure S9). A slight shift to higher frequencies observed in post-catalytic [Co^{II}-Fe^{II}], which was observed also in previous studies, can be attributed to the partial oxidation of iron ions from +2 to +3 during electrocatalysis.

XPS studies also confirm the remarkable stability of PB electrocatalysts. In order to investigate the oxidation state of electroactive Co^{II} sites in pristine and post catalytic electrodes Co2p signal was examined in the binding energy region between 810-775 eV. In previous studies the binding energy of Co2p$_{3/2}$ and Co2p$_{1/2}$ signals for Co^{II} salts have been reported as 782.28 and 798.38 eVs, respectively. For the pristine samples, Co2p$_{3/2}$

and Co2p$_{1/2}$ signals were observed in the same range. The similarity between the binding energies of Co2p signals obtained for pristine PBAs and previously reported Co^{II} salts suggests that the oxidation state of electroactive Co atoms is +2 (Figure 5). No significant changes in the Co2p$_{3/2}$ and Co2p$_{1/2}$ signals were observed in the post catalytic samples indicating the stability of the Co^{II} sites.
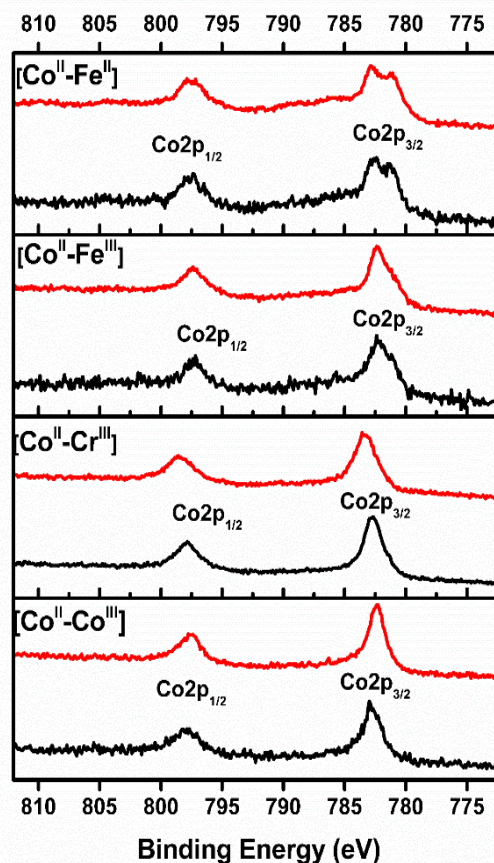

Figure 5. XPS of Co2p region for pristine (black lines) and post catalytic (red lines) of PB derivatives

In addition to Co2p, O1s signals were also examined for both pristine and post catalytic samples (Figure S10). The O1s signal whose binding energy is higher than 530 eV indicates the absence of any cobalt oxide species before and after electrochemical experiments even for [Co^{II}-Cr^{III}]. The observed values are displayed in Table S4. A mild noticeable broadening in the O1s signal in the post catalytic samples, indicating a partial and reversible oxidation of electroactive Co^{II} sites.

Mechanism for Catalytic Water Oxidation

The CN stretch could be considered as the fingerprint for cyanide-based coordination compounds. The comparison of the shift in the cyanide stretch can be used not only to confirm the bridging cyanide group but also to evaluate the oxidation states, and thus, electron densities of metal ions. Considering that the

cyanide stretch shifts to higher frequencies as the oxidation state of the metal increases a direct correlation can be established with the shift of the cyanide stretch and the electron deficiency of Co^{II} centers. The comparison of cyanide stretches implies that the electron densities of Co^{II} sites in Prussian blue analogues can be ordered as: $[Co^{II}-Co^{III}] \sim [Co^{II}-Cr^{III}] < [Co^{II}-Fe^{III}] < [Co^{II}-Fe^{II}]$ (Figure 6). This result is also in good agreement with the binding energies of Co2p orbitals obtained by XPS studies. The ordering of Co $2p_{3/2}$ peak is as $[Co^{II}-Co^{III}] > [Co^{II}-Cr^{III}] > [Co^{II}-Fe^{III}] > [Co^{II}-Fe^{II}]$, which points out that Co^{II} sites in $[Co^{II}-Co^{III}]$ analogue have the lowest electron densities among all. The evaluation of electron densities can give insight about the rate determining step (r.d.s.) in water oxidation catalysis. Two steps haven generally been reported to compete with each other as the r.d.s. in water oxidation process; i) $Co^{III}-OH/Co^{IV}-O$ (oxo) or $Co^{III}-OH/Co^{III}-O\bullet$ (oxyl) oxidation step and ii) the nucleophilic attack of water to the electrophilic oxygen atom of oxo/oxyl species that results in O–O bond formation. The increase in the electron density of Co^{II} site facilitates the former step while it decreases the electrophilic nature of oxo-intermediate and, thus, impedes the latter. The aforementioned discussion on the comparison of electron densities of Co^{II} sites in PBAs and their electrocatalytic performances clearly show that $[Co^{II}-Co^{III}]$ stands out as the most efficient catalyst among PBAs while it has Co^{II} sites with the lowest electron density. This correlation points out that the nucleophilic attack of water to
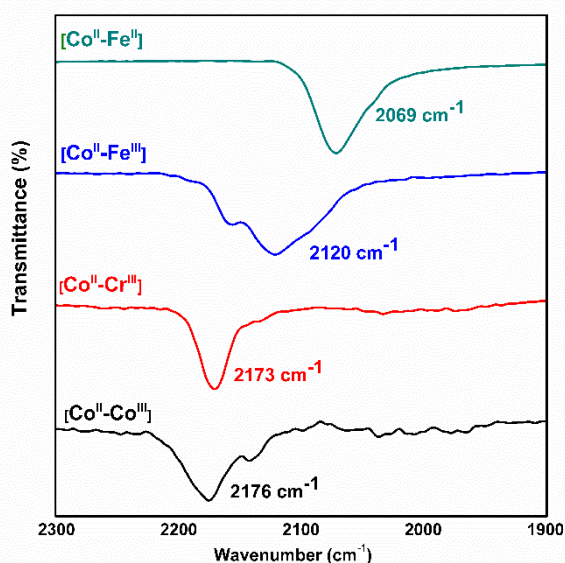

Figure 6. FTIR spectra of PB derivatives that shows cyanide stretches.

oxo/oxyl intermediate is the r.d.s. of water oxidation process for PBAs. Herein, it should be noted that the electronic properties of the catalysts will differ when a potential is applied. Catalytically active cobalt ions will be in their higher oxidation states particularly when the applied potential is above 1 V vs NHE. Nevertheless, the difference in the electron density of cobalt ions should be preserved given that structural integrity of cyanide

framework is preserved and that metal ion in $M(CN)_6$ building block is not oxidized. While this assumption can be valid with hexacyanometal groups that contain metal ions in their 3+ oxidation states, Fe^{2+} ion in $[Fe(CN)_6]^{4-}$ group is expected to be oxidized when a potential above 1 V is applied.[41] The oxidation of all Fe^{2+} ions is, however, a kinetically demanding process since it requires more potassium ions to be transported from the framework to the electrolyte due to charge neutrality and, more importantly, there are not enough potassium ions to produce a fully-oxidized $[Co^{II}-Fe^{III}]$ system. Therefore, the catalytically active species in $[Co^{II}-Fe^{II}]$ contains a mixture of Fe ions with oxidation states of 2+ and 3+. The difference in the curvatures of the bands assigned to $Fe^{2+/3+}$ and $Co^{2+/3+}$ redox processes for $[Co^{II}-Fe^{II}]$ and $[Co^{II}-Fe^{III}]$ also indicates different kinetics for these two analogues (Figure S11). The lower surface concentration and turnover frequency obtained for $[Co^{II}-Fe^{II}]$ could then be attributed to the difference in the kinetics of their electron transfer and their electronic properties.

A further analysis of the mechanism was made based on the Pourbaix diagram (Figure 7), which was obtained by performing CVs for $[Co^{II}-Co^{III}]$ at different pHs (Figure S12). The diagram shows that Co^{2+}/Co^{3+} redox process is pH dependent in the pH 4–10 range with a slope of 64 mV $log[H^+]^{-1}$, which refers to a $1H^+–1e^-$ process.
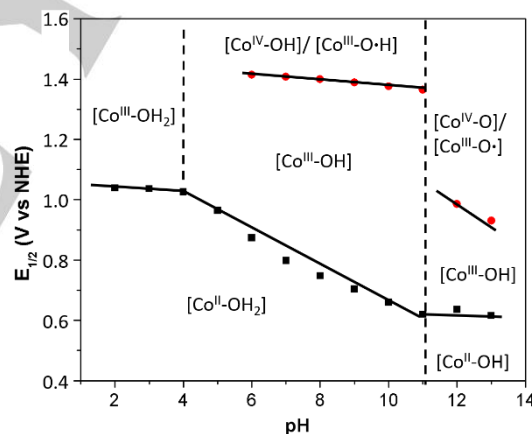

Figure 7. Pourbaix Diagram of $[Co^{II}-Co^{III}]$ in KPi buffer at pHs from 2 to 13. Cyclic Voltammograms that are recorded at these pHs are shown in Figure (S10).

Interestingly, the half-potential for the second redox step is preserved regardless of pH (<11), which indicates that a hydroxyl group is coordinated to the catalytically active Co^{IV}-oxo/Co^{III}-oxyl intermediate at neutral conditions. $[N_5Co^{IV}-OH]$ intermediate could undergo deprotonation in subsequent steps to form cobalt oxo/oxyl complex, followed by the nucleophilic attack of water to form a peroxo intermediate, which is one of the essential steps for O-O bond formation. A slightly different mechanism than the commonly-accepted mechanism for oxides was, thus, proposed for PBAs. The presence of additional bands in the CVs obtained above pH 11 suggests that water oxidation proceeds with a different mechanism in basic conditions.

Electronic Structure Calculations

In order to gain insight into the different performances of the PB analogues studied in this work, electronic structure calculations were performed with DFT.[37,38] (See SI for details) It is critical to understand the reason of rate enhancement through the Fe[II], Fe[III], Cr[III] and Co[III] cationic series that are used as the second metal separated by a cyanide bridge from the catalytically active Co site.

Oxidation of water would require the PCET steps to afford the formal Co[IV]–oxo/ Co[III]–O• moiety from the substrate bound aqua center with a +2 formal charge, i.e. Co[II](OH_2) → Co[III](OH) → Co[IV](O)/Co[III]–($O•$). Once the Co[IV](O) is accessed water attacks the Co[IV](O) to afford the O–O bond. This picture is in line with the existing mechanistic data in the literature.[39,42] Therefore, the structural and electronic properties of the Co[IV](O)/Co[III]–($O•$) center is the main focus of our quantum chemical calculations. It is important to note that there are no restrictions on the distribution of electrons in our calculation, thus formal assignments of Co[IV](O) or Co[III]–($O•$) for the Co center are less comprehensive levels of describing the Co–O bond compared to the completely delocalized (canonical) orbital picture given by the quantum chemical calculations.
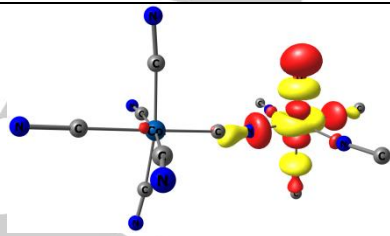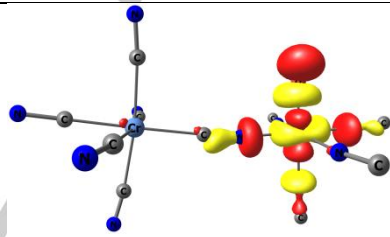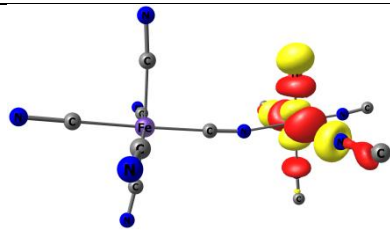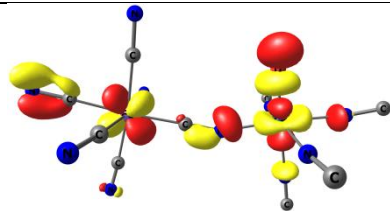
DFT calculations suggest that the catalytically active Co–O site is a local quartet and hence hosts three unpaired electrons. Depending on the nature of the neighbouring metal in a strong field environment, either one or zero electrons contribute to the total spin when a bimetallic model is considered as given in Table S5. The local quartet spin arrangement of the Co[IV] center is also verified by the spin density analysis as given in Table 2. Interestingly, the reactive Co[IV] center possesses a large degree of radical character distributed over the Co–O bond. Such electronic structure fingerprints of high valent Co moieties were recently shown to be related to reactivity,[43] where a seemingly Co(IV)=oxo species bearing a mixed electronic structure of the oxyl/oxo type was reported. In that work, one of us (Y.D.) has shown that, similar to the case reported in here, the oxo-wall[44] was indeed not broken and the local quartet spin arrangement, delocalized along the Co–O bond, showed substantial radical character on oxygen. Overall, a more appropriate electronic structure assignment for the *in situ* generated, catalytically competent, O–O bond forming species is a mixed Co–oxo/oxyl.

CN stretching frequencies (ν(CN)) and molecular orbitals were investigated to enlighten the molecular reasons of catalytic activity (Table 2).

The calculated trend of ν(CN) is in good agreement with experimental results and show the flow of electron density from the Co site. More importantly the critical O–O bond formation step is well understood by analyzing the attack of water to the Co–O center. The oxygen lone pairs possessed by water are seeking empty orbitals on the Co–O center for which the best candidate is the LUMO. As shown in Table S5, the σ* MO generated from Co_d and O_p contributions is obtained at lower energies (E_{LUMO} in Table 2) through the Fe[II], Fe[III], Cr[III], and Co[III] sites. Thus the electron affinity of Co[IV]–O center is increased, the attack of water became more facile and hence the lower overpotentials measured in our electrochemical experiments. Our quantum chemical calculations thus show that the reactive Co–oxo/oxyl center possesses a local quartet spin arrangement. Two of the three quartet spin electrons are distributed over Co and one over oxygen however all three electrons are better described to share Co_d and O_p orbitals through the Co–O bond. The reactivity correlates with obtaining the LUMO, to be attacked by incoming water, at lower energies as summarized in Figure 8. Note that the truncated quantum chemical model might not capture all the structural features of the PB surface yet it is a good compromise between accuracy and cost. Moreover with the assistance of the experimental data, the electronic structure assignment of the active species being CoIV(O)/CoIII–(O•) could be made, and hence the model chemistry is useful.

Table 2. Structural and Electronic Properties of the M/Co PBAs Computed at UM06L/cc-pVTZ Level of Theory[a]

[Co[II]-Co[III]]	
	R Co–O (Å) 1.652
	ν CN (cm^{-1}) 2195
	ρ (O) 1.22
	ρ (Co[IV]) 1.63
	E_{LUMO} (eV) -14.34

[Co[II]-Cr[III]]	
	R Co–O (Å) 1.654
	ν CN (cm^{-1}) 2158
	ρ (O) 1.24
	ρ (Co[IV]) 1.62
	E_{LUMO} (eV) -13.85

[Co[II]-Fe[III]]	
	R Co–O (Å) 1.653
	ν CN (cm^{-1}) 2160
	ρ (O) 1.23
	ρ (Co[IV]) 1.62
	E_{LUMO} (eV) -12.91

[Co[II]-Fe[II]]	
	R Co–O (Å) 1.684
	ν CN (cm^{-1}) 2114
	ρ (O) 1.17
	ρ (Co[IV]) 2.10
	E_{LUMO} (eV) -11.06

a Surfaces were generated at 0.05 au.

Conclusions

Previous electrochemical studies on Prussian blue analogues have shown that having a cobalt site coordinated to nitrogen atoms of cyanide bridging group is essential to obtain efficient PBA electrocatalysts for water oxidation. Herein, a series of cobalt hexacyanometalates with a general formula of $K_aCo_b[M(CN)_6]$ ($M:Co^{III}$, Cr^{III}, and $Fe^{II/III}$) have been prepared to investigate the effect of hexacyanometal group to the electrocatalytic activity of CHCMs. Tafel analysis and chronoamperometry experiments reveal that $[Co^{II}-Co^{III}]$ serves as the most efficient electrocatalyst for water oxidation among the CHCMs studied. Infrared and XPS studies indicate that it has the Co(II) center with the lowest electron density, which is also confirmed by DFT studies.

Overall, experimental and computational studies lead to the following conclusions:

i) Electron density of Co^{2+} is a decisive electronic criterion for achieving efficient water oxidation electrocatalysis and this parameter could be tuned by changing the type of hexacyanometal group.

ii) The electron density of Co(II) can be reduced by increasing the oxidation state of the metal ion of $[M(CN)_6]^{n-}$ group.

iii) Electrophilicity of the $Co^{IV}-O$ center can be probed by molecular orbital analysis and might be a useful tool for realization of new PBAs bearing reactive Co species as potent WOCs.

iv) Nucleophilic attack of water to the cobalt-oxo intermediate should be the rate determining step for water oxidation catalysis with Prussian blue analogues.

v) Theoretical calculations show that O–O bond forming species has a mixed Co–oxo/oxyl character.
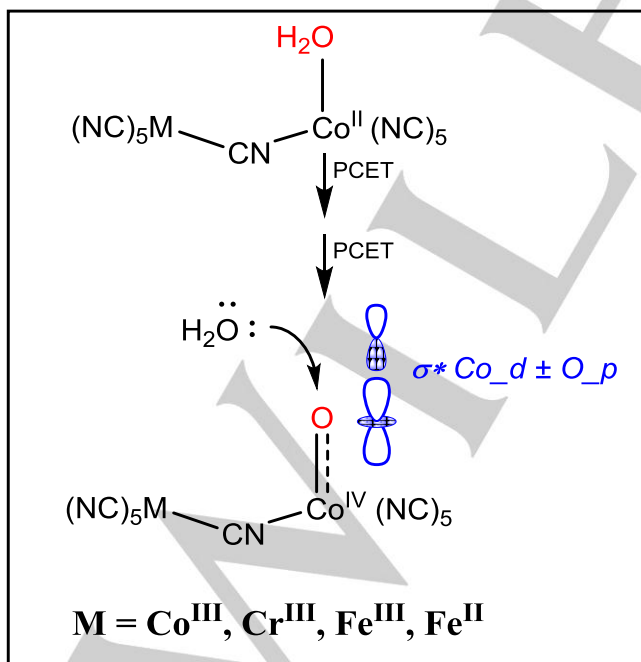

Figure 8. O–O bond formation at the $Co^{IV}-O$ center.

In conclusion, the following mechanism has been proposed based on the experimental and computational studies (Figure 9). This study shows that electronic properties, thus, the electrocatalytic activity of catalytically active cobalt site can easily be tuned using the versatile chemistry of PBAs and neighbouring metal ions should also be considered as an important parameter to evaluate the catalytic activities of water oxidation electrocatalysts. Detailed electronic structure calculations employing multi-reference techniques about various Co–O systems are under way to corroborate the nature of the $Co^{IV}-O$ bonding and reactivity.
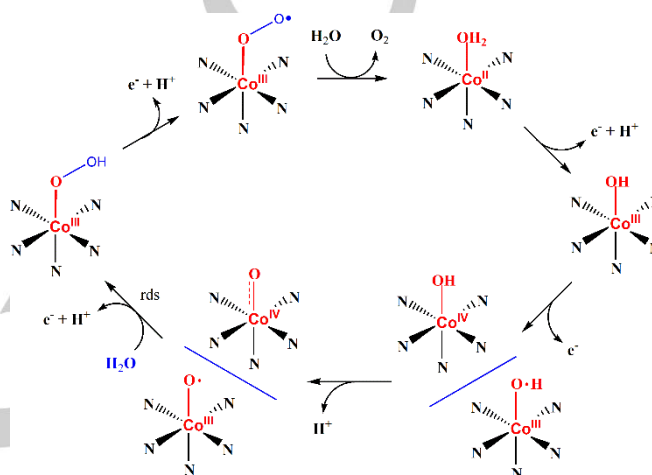

Figure 9. Proposed mechanism for water oxidation process for PBAs.

Experimental Section

Chemicals and solutions

Potassium hexacyanocobaltate $K_3[Co(CN)_6]$ (Sigma-Aldrich, >97.0%), cobalt chloride hexahydrate $CoCl_2.6H_2O$ (Sigma-Aldrich, 98.0%), Potassium hexacyanochromate $K_3[Cr(CN)_6]$ (Aldrich, 99.99%), Potassium hexacyanoferrate $K_3[Fe(CN)_6]$ (Sigma-Aldrich, >97.0%), potassium hexacyanoferrate trihydrate, $K_3[Fe(CN)_6].3H_2O$ (Sigma-Aldrich, 98.5-102%). All the solutions were prepared with Millipore Milli-Q deionized water with a resistivity of 18.2 mΩ.cm.

Experimental

$K_aCo_b[M(CN)_6]\cdot xH_2O$ ($M = Fe^{II}$, Fe^{III}, Co^{III}, and Cr^{III}) abbreviated throughout as $[Co^{II}-Fe^{II}]$, $[Co^{II}-Fe^{III}]$, $[Co^{II}-Co^{III}]$, and $[Co^{II}-Cr^{III}]$. In the case of $[Co^{II}-Co^{III}]$ an aqueous solution of $CoCl_2.6H_2O$ (0.15 M, 20 mL) was added dropwise to an aqueous solution of $K_3[Co(CN)_6]$ (0.10 M, 20 mL) at room temperature. The mixture was kept under stirring for 1 hour and then allowed to wait overnight for precipitation. The solution was filtered by vacuum suction and washed with copious amounts of water to obtain the pink powder. The powder was dried further in desiccator. The same procedure was applied for $[Co^{II}-Fe^{II}]$ (dark blue), $[Co^{II}-Fe^{III}]$ (dark brown), and $[Co^{II}-Cr^{III}]$ (pale yellow).

Preparation PBA modified FTO Electrodes

FTO electrodes were procured from Sigma-Aldrich (with ~80% transmittance, 2 mm with a surface resistance of 7 Ω.sq^{-1}, 1x2 cm). Electrodes were washed by sonication for 10 minutes in basic soapy solution, deionized water and isopropanol respectively. Then they were annealed at 400 °C for 30 minutes. Catalyst modified electrodes were

prepared by drop casting method. A mixture of 5 mg of PBA catalyst, 500 µL DMF, 500 µL water and 100 µL Nafion solution were mixed and sonicated for 30 minutes. After making a stable suspension, 50 µL of it was taken and dropped onto by covering 1 cm^2 of the FTO electrode. Electrodes were then dried at room temperature for 10 minutes followed by 80 ^{o}C for 10 minutes in an oven. Then they were left in desiccator until further use for electrochemical experiments and characterization.

Electrochemical Measurements

Gamry Instruments Interface 1000 Potentiostat/Galvanostat was used for performing electrochemical measurements. A conventional three electrode cell was used with Ag/AgCl (3.5 M KCl) as reference electrode, FTO as the working electrode, and Pt wire as counter electrode. YSI 5100 dissolved oxygen sensing electrode instrument equipped with a dissolved oxygen field probe was used to determine the oxygen evolution. KPi buffer solution was prepared by using KH_2PO_4 and K_2HPO_4 and pH of the solution was adjusted by adding H_3PO_4 or KOH. Bulk water electrolysis was performed with a two compartment cell with separation of a glass frit. The electrolysis and steady state chronoamperometry experiments were performed in KPi buffer solution containing 1 M KNO_3 as supporting electrolyte. Mettler Toledo S220 SevenCompact™ pH/Ion pH meter was used to determine the pHs of buffer solutions. All of the electrochemical experiments were performed at room temperature and under N_2 atmosphere.

Physical Measurements

XRD patterns were measured by using a Pananalytical X'PertPro Multipurpose X-Ray Diffractometer (MPD) with CuK$_\alpha$ X- Ray Radiation (λ= 1.5418 Å). GI-XRD patterns were recorded by using a Panalytical X'Pert3 MRD Material Research Diffractometer (MRD) with CuK$_\alpha$ X-ray radiation (l=1.5418 a) at an incident (w) angle of 0.58. FTIR spectra were taken by using a Bruker Alpha Platinum-ATR Spectrometer with wavenumber range between 4000-400 cm^{-1}. FEI-Quanta 200 FEG ESEM was used for imaging and EDAX analysis, at 5 kV beam voltage for imaging and 30 kV for EDAX. XPS analysis was performed using Thermo Scientific K-Alpha X-Ray Photoelectron Spectrometer system with a AlK$_\alpha$ microfocused monochromator source operating at 400 mm spot size and $h\gamma$= 14.86.6 eV accompanied by a flood gun, 200 eV for survey scan and 30 eV for individual scans. In order to plot and analyze the results Origin Pro 8.5 was used.

Acknowledgements

[1]   N. S. Lewis, D. G. Nocera, *PNAS* **2006**, *103*, 15729–15735.

[2]   A. Llobet, F. Meyer, *Angew. Chemie - Int. Ed.* **2011**, *50*, A30–A33.

[3]   N. S. Lewis, *Science (80-.).* **2016**, *351*, aad1920-9.

[4]   J. Marshall, *Nature* **2014**, *510*, 22–24.

[5]   J. R. McKone, N. S. Lewis, H. B. Gray, *Chem. Mater.* **2014**, *26*, 407–414.

[6]   M. G. Walter, E. L. Warren, J. R. McKone, S. W. Boettcher, Q. Mi, E. A. Santori, N. S. Lewis, *Chem. Rev.* **2010**, *110*, 6446–6473.

[7]   K. J. Young, L. A. Martini, R. L. Milot, R. C. Snoeberger, V. S. Batista, C. A. Schmuttenmaer, R. H. Crabtree, G. W. Brudvig, *Coord. Chem. Rev.* **2012**, *256*, 2503–2520.

[8]   M. E. G. Lyons, M. P. Brandon, *J. Electroanal. Chem.* **2010**, *641*, 119–130.

[9]   R. D. L. Smith, M. S. Prévot, R. D. Fagan, Z. Zhang, P. A. Sedach, M. K. J. Siu, S. Trudel, C. P. Berlinguette, *Science (80-.).* **2013**, *340*, 60–63.

[10]   Y. Surendranath, M. Dinca, D. G. Nocera, *J. Am. Chem. Soc.* **2009**, *131*, 2615–2620.

[11]   S. Jung, C. C. L. McCrory, I. M. Ferrer, J. C. Peters, T. F. Jaramillo, *J. Mater. Chem. A* **2016**, *4*, 3068–3076.

[12]   C. C. L. McCrory, S. Jung, I. M. Ferrer, S. M. Chatman, J. C. Peters, T. F. Jaramillo, *J. Am. Chem. Soc.* **2015**, *137*, 4347–4357.

[13]   Gurudayal, D. Sabba, M. H. Kumar, L. H. Wong, J. Barber, M. Grätzel, N. Mathews, *Nano Lett.* **2015**, *15*, 3833–3839.

[14]   A. Kudo, H. Kato, S. Nakagawa, *J. Phys. Chem. B* **2000**, *104*, 571–575.

[15]   J. Suntivich, K. J. May, H. A. Gasteiger, J. B. Goodenough, Y. Shao-Horn, *Science (80-.).* **2011**, *334*, 1383–1385.

[16]   Y. Zhang, C. Zhao, X. Dai, H. Lin, B. Cui, J. Li, *J. Power Sources* **2013**, *243*, 908–912.

[17]   L. G. Bloor, P. I. Molina, M. D. Symes, L. Cronin, *J. Am. Chem. Soc.* **2014**, *136*, 3304–3311.

[18]   T. Reier, M. Oezaslan, P. Strasser, *ACS Catal.* **2012**, *2*, 1765–1772.

[19]   B. Nepal, S. Das, *Angew. Chemie Int. Ed.* **2013**, *52*, 7224–7227.

[20]   Y. Gong, Z. Hao, J. Meng, H. Shi, P. Jiang, M. Zhang, J. Lin, *Chempluschem* **2014**, *79*, 266–277.

[21]   Y. Matsumoto, E. Sato, *Mater. Chem. Phys.* **1986**, *14*, 397–426.

[22]   D. E. Hall, *J. Electrochem. Soc.* **1985**, *132*, 41C–48C.

[23]   J. R. Galan-Mascaros, *ChemElectroChem* **2015**, *2*, 37–50.

[24]   C. C. L. McCrory, S. Jung, J. C. Peters, T. F. Jaramillo, *J. Am. Chem. Soc.* **2013**, *135*, 16977–16987.

[25]   Z. Chen, A. R. Rathmell, S. Ye, A. R. Wilson, B. J. Wiley, *Angew. Chemie Int. Ed.* **2013**, *52*, 13708–13711.

[26]   D. Ressnig, M. Shalom, J. Patscheider, R. Moré, F. Evangelisti, M. Antonietti, G. R. Patzke, *J. Mater. Chem. A* **2015**, *3*, 5072–5082.

[27]   S. V. K. Nune, A. T. Basaran, E. Ülker, R. Mishra, F. Karadas, *ChemCatChem* **2017**, *9*, 300–307.

[28]   S. Pintado, S. Goberna-Ferron, E. C. Escudero-Adan, J. R. Galan-

Mascaros, *J. Am. Chem. Soc.* **2013**, *135*, 13270–13273.

[29]   F. Hegner, I. Herraiz-Cardona, D. Cardenas-Morcoso, N. Lopez, J. R. Galan-Mascaros, S. Gimenez, *ACS Appl. Mater. Interfaces* **2017**, DOI 10.1021/acsami.7b09449.

[30]   F. Hegner, D. C.-M. Cardenas-Morcoso, S. Gimenez, N. Lopez, J. R. Galan-Mascaros, *ChemSusChem* **2017**, DOI 10.1002/cssc.201701538.

[31]   S. Goberna-Ferron, W. Y. Hernadez, B. Rodríguez-García, J. R. Galan-Mascaros, *ACS Catal.* **2014**, *4*, 1637–1641.

[32]   M. Aksoy, S. V. K. Nune, F. Karadas, *Inorg. Chem.* **2016**, *55*, 4301–4307.

[33]   L. Han, P. Tang, Á. Reyes-Carmona, B. Rodríguez-García, M. Torréns, J. R. Morante, J. Arbiol, J. R. Galan-Mascaros, *J. Am. Chem. Soc.* **2016**, *138*, 16037–16045.

[34]   Y. Yamada, K. Oyama, R. Gates, S. Fukuzumi, *Angew. Chem.* **2015**, *127*, 5705–5709.

[35]   Y. Yamada, M. Yoneda, S. Fukuzumi, *Chem. - A Eur. J.* **2013**, *19*, 11733–11741.

[36]   Y. Yamada, K. Oyama, T. Suenobu, S. Fukuzumi, S. Fukuzumi, W. Nam, R. Sarangi, S. Fukuzumi, W. Nam, Y. Xie, et al., *Chem. Commun.* **2017**, *53*, 3418–3421.

[37]   W. Kohn, A. D. Becke, R. G. Parr, *J. Phys. Chem.* **1996**, *100*, 12974–12980.

[38]   R. G. Parr, W. Yang, *Density-Functional Theory of Atoms and Molecules*, Oxford University Press, New York, **1989**.

[39]   D. J. Wasylenko, C. Ganesamoorthy, J. Borau-Garcia, C. P. Berlinguette, *Chem. Commun.* **2011**, *47*, 4249–4251.

[40]   K. Nakamoto, *Infrared and Raman Spectra of Inorganic and Coordination Compounds Part B: Applications in Coordination, Organometallic, and Bioinorganic Chemistry*, John Wiley & Sons, Inc., **2009**.

[41]   R. O. Lezna, R. Romagnoli, N. R. de Tacconi, K. Rajeshwar, *J. Phys. Chem. B* **2002**, *106*, 3612–3621.

[42]   D. W. Crandell, S. Ghosh, C. P. Berlinguette, M.-H. Baik, *ChemSusChem* **2015**, *8*, 844–852.

[43]   B. Wang, Y.-M. Lee, W.-Y. Tcho, S. Tussupbayev, S.-T. Kim, Y. Kim, M. S. Seo, K.-B. Cho, Y. Dede, B. C. Keegan, et al., *Nat. Commun.* **2017**, *8*, 14839.

[44]   B. Wang, Y.-M. Lee, W.-Y. Tcho, S. Tussupbayev, S.-T. Kim, Y. Kim, M. S. Seo, K.-B. Cho, Y. Dede, B. C. Keegan, et al., *Nat. Commun.* **2017**, *8*, 14839.

FULL PAPER

Entry for the Table of Contents (Please choose one layout)

FULL PAPER
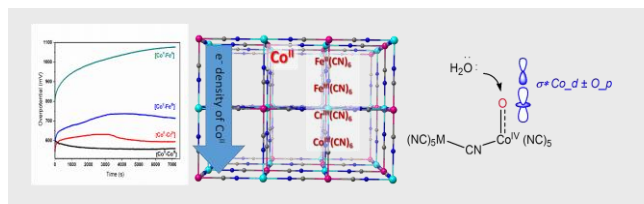
The effect of electroinactive hexacyanometal group to electroactive Co(II) site in Prussian Blue analogues was probed by experimental and computational studies.

E. P. Alsaç, E. Ülker, S. V. K. Nune, Y. Dede,* F. Karadas *

Page No. – Page No.

Title